International Journal of
Automotive Manufacturing and Materials (IJAMM)

Scilight

Article

Gasoline Particulate Filter Diagnosis Strategy Based on Correlation Coefficients

Naishang Deng, Tonghao Song, Pengyuan Sun *, and Rongyong Ma

General Research and Development Institute, China FAW Corporation Limited, Changchun 130011, China
* Correspondence: sunpengyuan@faw.com.cn
Received: 29 September 2025; Revised: 4 January 2026; Accepted: 25 March 2026; Published: 2 April 2026

Abstract: This paper presents a monitoring approach for Gasoline Particulate Filter (GPF) systems. Initially, two correlation coefficients are computed: one is between the differential pressure across the GPF and the exhaust gas volume flow rate, and the other is between the differential pressure across the muffler and the exhaust gas volume flow rate. Subsequently, the failure mode of the GPF system is identified by analyzing the distribution of these two correlation coefficients in a two-dimensional coordinate plane, where the former coefficient serves as the horizontal axis and the latter as the vertical axis. The proposed strategy was implemented in an automotive-grade controller, and on-vehicle validation tests were conducted under both the Worldwide Harmonized Light-Duty Vehicle Test Cycle (WLTC) and real-road driving conditions. The test results demonstrate that this method can accurately detect multiple failure modes, including GPF catastrophic failure, and interchange or disconnection of the GPF differential pressure sensor, thereby satisfying the requirements of worldwide OBD standards which mainly include EOBD (European On-Board Diagnostics), OBDII (On-Board Diagnostics II) and COBD (Chinese On-Board Diagnostics). Furthermore, this approach obviates the need for vehicle-level calibration of the GPF differential pressure-volume flow rate characteristic model and the muffler differential pressure-volume flow rate characteristic model. This not only reduces the consumption of resources such as prototype vehicles and chassis dynamometers but also shortens the overall development cycle time.

Keywords: onboard diagnostic system (OBD); gasoline particulate filter (GPF); correlations; monitoring strategy

1. Introduction

Gasoline Particulate Filters (GPFs) effectively reduce particulate matter (PM) and particle number (PN) in vehicle exhaust. Equipping light-duty vehicles with GPFs is a critical measure to comply with increasingly stringent worldwide emission standards [1–5].

On-Board Diagnostic (OBD) system must be capable of detecting a malfunction when there is GPF catastrophic failure, or implausible signal failures in GPF-associated sensors [6–8]. For the detection of GPF catastrophic failure, two primary approaches are currently dominant: one based on the temperature differential between the upstream and downstream of the GPF, and the other based on the pressure differential across the GPF. Owing to cost constraints, the pressure differential-based approach is more widely adopted in engineering practices. Liu et al. [9] proposes a diagnostic strategy that constructs a neural network dataset using the upstream-downstream pressure differential of the GPF under steady-state operating conditions, with validation performed on an engine test bench [9], however, this method poses challenges for implementation in embedded controllers. Wang et al. [10] presents a diagnostic strategy that calculates the GPF carrier characteristic factor using the deviation between measured and model-predicted pressure differentials under dynamic operating conditions, with verification conducted via on-vehicle tests [10], this method, nonetheless, requires the establishment of a GPF upstream-downstream pressure differential model. While, in current production applications, the detection of GPF catastrophic failure is typically accomplished by comparing the measured upstream-downstream pressure differential of the GPF with the model-estimated pressure differential. That said, the development of such a GPF upstream-downstream pressure differential model necessitates an extensive volume of vehicle test data, resulting in a substantial development workload.

2. Basic Knowledge of GPF Monitoring Technology

2.1. Differential Pressure-Flow Characteristics of GPF and Muffler

The structure of the Gasoline Particulate Filter (GPF) system is illustrated in Figure 1. Among its components, the GPF differential pressure sensor is a dual-diaphragm sensor. Based on this sensor, three parameters can be measured: the exhaust gas pressure upstream of the GPF, the exhaust gas pressure downstream of the GPF, and the exhaust gas pressure difference between the upstream and downstream of the GPF (hereafter referred to as "GPF differential pressure"). The exhaust gas pressure difference between the upstream and downstream of the muffler is the difference between the exhaust gas pressure downstream of the GPF and ambient pressure (hereafter referred to as "muffler differential pressure"). And the ambient pressure can be measured based on the sensor integrated on engine control module as shown in Figure 1.

In accordance with OBD standards, it is required to monitor two types of failures: GPF catastrophic failure and implausible signal failures of the GPF differential pressure sensor. In engineering practices, the monitoring of GPF catastrophic failure relies on the GPF differential pressure. Meanwhile, the main causes of implausible output signals from the GPF differential pressure sensor include the disconnection of the upstream pressure hoseline, the disconnection of the downstream pressure hoseline, or the interchange of the upstream and downstream pressure hoseline. To meet regulatory requirements and provide support for after-sales maintenance, these failure modes need to be monitored. In addition, OBD standards require the diagnosis of circuit continuity failures in differential pressure sensors. Mature technical solutions for these (failures) already exist, but they are not covered in this paper.

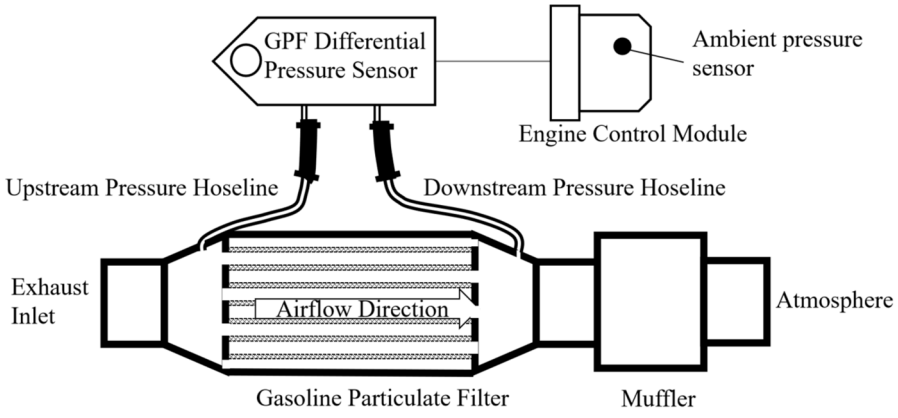

Figure 1. Schematic Diagram of GPF Monitoring Strategy.

When exhaust gas flows through the GPF carrier, a pressure difference (i.e., GPF differential pressure) exists between the upstream and downstream of the carrier, resulting from the frictional loss (including permeation loss) and compression/expansion loss of the gas flow, as illustrated in Figure 2. Specifically, the frictional loss is proportional to the exhaust gas volume flow rate, while the compression/expansion loss is proportional to the square of the exhaust gas volume flow rate [11].

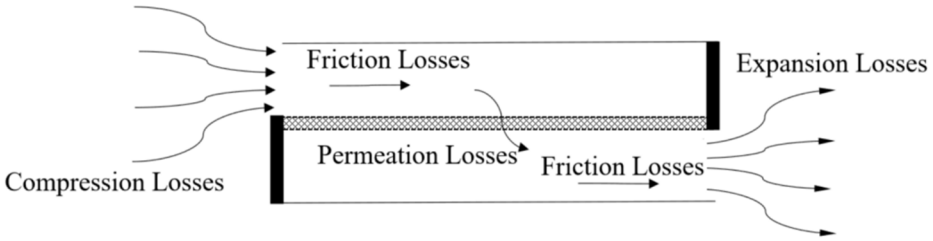

Figure 2. Schematic diagram of GPF Pressure Drop through GPF Carrier.

The relationship between GPF differential pressure (ΔP_{GPF}) and exhaust gas volume flow rate (Q) can be described as [12]:

$$\Delta P_{GPF} = AQ + BQ^2 \quad (1)$$

In the formula, ΔP_{GPF} denotes the GPF differential pressure, Q denotes the exhaust gas volume flow rate, A denotes the frictional loss coefficient, B denotes the compression/expansion loss coefficient. Coefficients A and B are related to the intrinsic characteristics of the GPF carrier and the gas state inside the GPF, and their values need to be determined through experiments.

Figure 3 illustrates the GPF differential pressure (ΔP_{GPF})-volume flow rate (Q) characteristics under various failure modes from real-vehicle tests. Among the data presented, the differential pressure values are the measured values from the sensor, while the exhaust gas volume flow rate (Q) is estimated using Equation (2).

$$Q = M * R * T/P/M_{air} \tag{2}$$

In the equation, M represents the exhaust gas mass flow rate, T represents the internal temperature of the GPF, P represents the internal pressure of the GPF, R represents the ideal gas constant, M_{air} represents the molecular weight of air, which is 28.9.

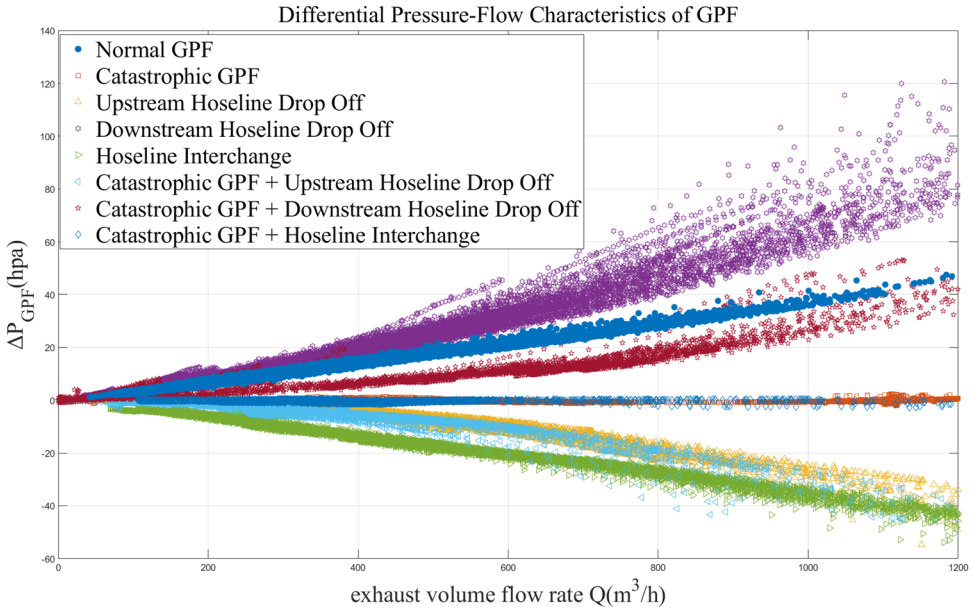

Figure 3. Differential Pressure-Flow Characteristics of GPF in each Failure Mode.

The ΔP_{GPF}-Q datasets of "Normal GPF" mode can be clearly distinguished from that of "Catastrophic GPF" mode, "Upstream Hoseline Drop Off" mode, "Hoseline Interchange" mode, "Catastrophic GPF & Upstream Hoseline Drop Off" mode and "Catastrophic GPF & Hoseline Interchange" mode. But it can neither be clearly distinguished from that of "Downstream Hoseline Drop Off" mode nor "Catastrophic GPF & Downstream Hoseline Drop Off" mode as shown in Figure 3. So, the OBD system can't detect a malfunction when downstream hoseline drop off, even if a GPF catastrophic failure exists. This could be used to evade OBD monitoring. It's not allowed by the OBD standards.

Similarly, the relationship between the muffler differential pressure ($\Delta P_{muffler}$) and the exhaust gas volume flow rate (Q) can be described as:

$$\Delta P_{muffler} = CQ + DQ^2 \tag{3}$$

In the formula, $\Delta P_{muffler}$ denotes the muffler differential pressure, C denotes the frictional loss coefficient, D denotes the compression/expansion loss coefficient. Coefficients C and D are associated with the characteristics of the exhaust pipe downstream of the GPF carrier and the gas state of the exhaust gas. Their specific values need to be determined through experimental testing.

Figure 4 illustrates the muffler differential pressure ($\Delta P_{muffler}$)-volume flow rate (Q) characteristics under various failure modes from real-vehicle tests. Fortunately, the ΔP_{muffle}-Q datasets of "Normal GPF" mode can be clearly distinguished from that of "Downstream Hoseline Drop Off" mode and "Catastrophic GPF & Downstream Hoseline Drop Off" mode. When both the ΔP_{GPF}-Q datasets and the $\Delta P_{muffler}$-Q datasets are used, it has no chance that the OBD system detects no malfunction when a GPF catastrophic failure exists.

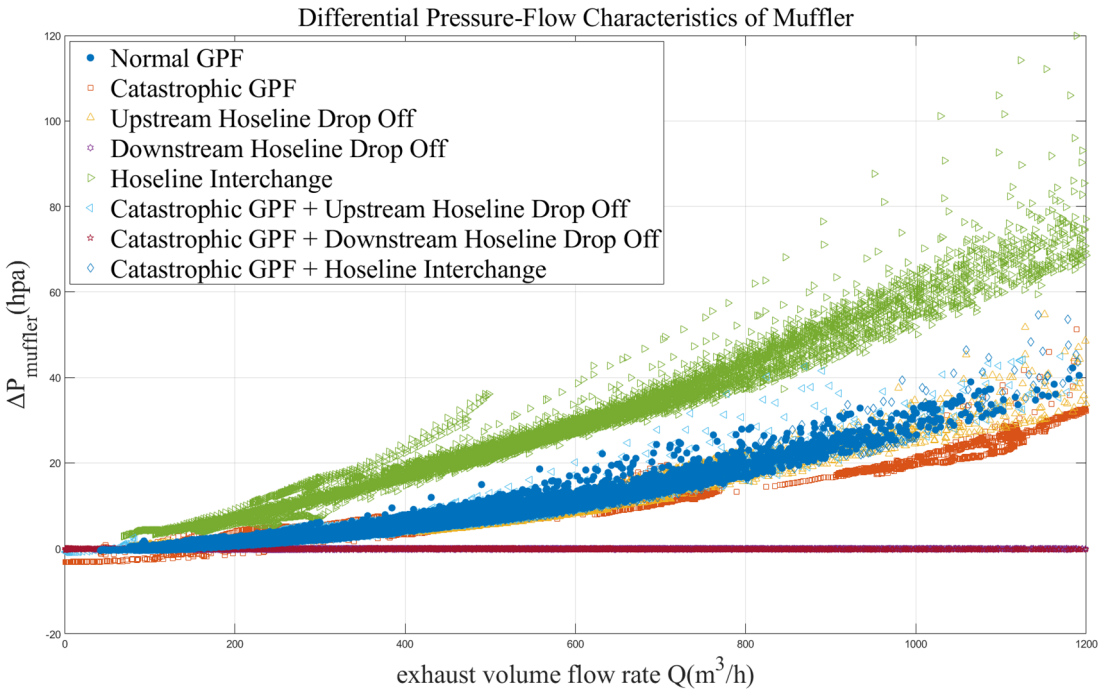

Figure 4. Differential Pressure-Flow Characteristics of Muffler in each Failure Mode.

Measured data indicate that there is no deterministic relationship between differential pressure ($\Delta P_{GPF}/\Delta P_{muffler}$) and exhaust flow rate (Q). This is attributed to multiple error factors in the system, primarily including:

(1) Inherent measurement errors of the GPF differential pressure (ΔP_{GPF}) sensor itself;
(2) Errors in the exhaust gas mass flow rate(M) calculated by the charging model (approximately ±5% in engineering practice);
(3) The temperature (T) at different locations inside the GPF carrier is not a fixed value and cannot be accurately obtained;
(4) The pressure (P) at different locations inside the GPF is not a fixed value and cannot be accurately obtained;
(5) The chemical composition of the exhaust gas is not fixed and can only be estimated approximately.

If diagnosis is to be performed based on the modeled differential pressure and actual differential pressure, it is necessary to ensure the differential pressure model has sufficient accuracy. This requires establishing a relatively complex model and determining the influence of various factors through extensive real-vehicle tests, which results in significant consumption of test resources and heavy development workload. It needs almost two days calibration work on chassis dynamometers and few weeks real road test. Therefore, there is a need to explore a new diagnosis method that does not rely on a differential pressure model. Based on this, this paper presents a GPF monitoring strategy based on correlation coefficients, details of which are as follows.

2.2. GPF Monitoring Strategy Based on Correlation Coefficients

As evidenced by the aforementioned real-vehicle test data, while no deterministic relationship exists between the measured values of GPF differential pressure/muffler differential pressure and exhaust flow rate, both exhibit a correlational relationship with exhaust flow rate. On this basis, it is feasible to explore the diagnosis of GPF catastrophic failure and implausible differential pressure sensor signal failures using correlation coefficients.

Commonly employed correlation coefficients in engineering practice include the Pearson product-moment correlation coefficient, Spearman's rank correlation coefficient, and Kendall's rank correlation coefficient. Their respective application scenarios are as follows:

(1) The Pearson product-moment correlation coefficient is primarily utilized to quantify the degree of linear correlation between two continuous variables that conform to a normal distribution;
(2) Kendall's rank correlation coefficient is typically applied to assess the ordinal association between two ordinal categorical variables or continuous variables transformed into ordinal ranks;

(3) Spearman's rank correlation coefficient conducts linear correlation analysis based on the rank order of two variables, and it imposes no constraints on the distribution characteristics of the original variables-rendering it robust to non-normal data and outliers.

As indicated in Equation (1), a quadratic relationship exists between differential pressure and volume flow rate. Consequently, compared with the other two correlation coefficients, Spearman's rank correlation coefficient enables a more rational evaluation of the correlational relationship between differential pressure and volume flow rate. Its mathematical expression is provided below:

$$\rho = 1 - \frac{6\Sigma\, d_i^2}{n(n^2-1)} \tag{4}$$

In the formula, d_i represents the difference between the ranks of each pair of samples from the two variables, n denotes the sample size [13].

Based on the test data presented in Figures 3 and 4, the correlation coefficients ρ_{GPF} (for the ΔP_{GPF}-Q pair) and $\rho_{muffler}$ (for the $\Delta P_{muffler}$-Q pair) were calculated for each mode. The calculation results are provided in Table 1 and Figure 5.

Table 1. Spearman Rank Correlation Coefficients in Each Failure Mode.

Failure Mode	ρ_{GPF}	$\rho_{muffler}$	Range	Sample Size
Normal GPF	0.9952	0.9421	Range1	19,298
Catastrophic GPF	−0.3630	0.6987	Range3	41,850
Upstream Hoseline Drop Off	−0.9751	0.9750	Range4	150,599
Downstream Hoseline Drop Off	0.9937	0.0166	Range2	215,875
Hoseline Interchange	−0.9971	0.9958	Range4	124,984
Catastrophic GPF & Upstream Hoseline Drop Off	−0.9481	0.9492	Range4	108,335
Catastrophic GPF & Downstream Hoseline Drop Off	0.9604	−0.2799	Range2	45,040
Catastrophic GPF & Hoseline Interchange	−0.2488	0.9878	Range3	59,711

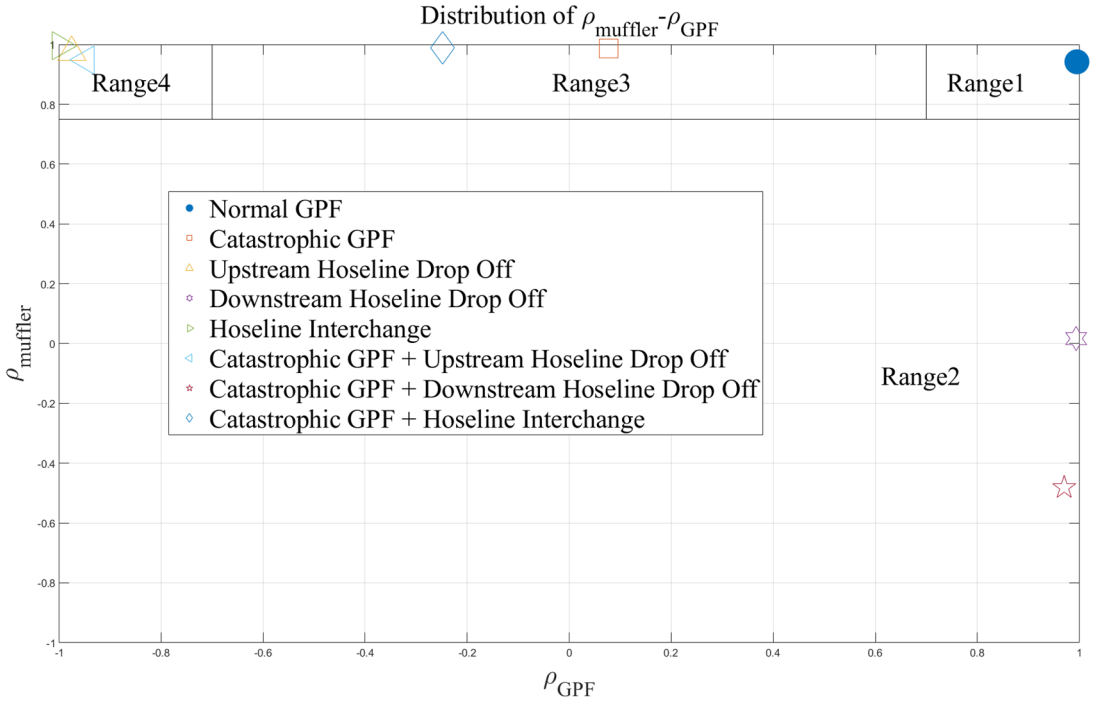

Figure 5. Distribution of $\rho_{muffler}$-ρ_{GPF} in each Failure Mode.

It is evident from the analysis that a distinct distinguishability exists between the normal and failures of the GPF system. Specifically, both the presence of a failure in the GPF system and the specific failure mode can be identified by analyzing the distribution of $\rho_{muffler}$-ρ_{GPF} coordinate points within the two-dimensional plane. A comprehensive summary of the diagnostic criteria and corresponding failure mode is presented in Table 2.

Table 2. $\rho_{muffler}$-ρ_{GPF} Distribution Ranges and Corresponding Failure Modes.

Range	Distribution of $\rho_{muffler}$	Distribution of ρ_{GPF}	Failure Modes
Range1	$\rho_{muffler} \in (0.75, 1]$	$\rho_{GPF} \in (0.7, 1]$	GPF Normal
Range2	$\rho_{muffler} \in [-1, 0.75]$	Not care	GPF Downstream Hoseline Drop Off
Range3	$\rho_{muffler} \in (0.75, 1]$	$\rho_{GPF} \in (-0.7, 0.7]$	Catastrophic GPF
Range4	$\rho_{muffler} \in (0.75, 1]$	$\rho_{GPF} \in [-1, -0.7]$	GPF Upstream Hoseline Drop Off / Hoseline Interchange

3. GPF Monitoring Strategy Development in Vehicle

While diagnosis based on the ρ_{GPF}-$\rho_{muffler}$ distribution is feasible, calculating ρ_{GPF} and $\rho_{muffler}$ requires collecting a large number of data points for ΔP_{GPF}, $\Delta P_{muffler}$, *and* Q. Due to the performance limitations of automotive-grade MCU (Micro-controller Unit), it is not possible to cache all ΔP_{GPF}, $\Delta P_{muffler}$, *and* Q data generated during vehicle operation. Therefore, it is necessary to design the specific implementation method of the diagnosis based on automotive-grade MCU. Figure 6 illustrates the diagnostic strategy proposed in this paper.

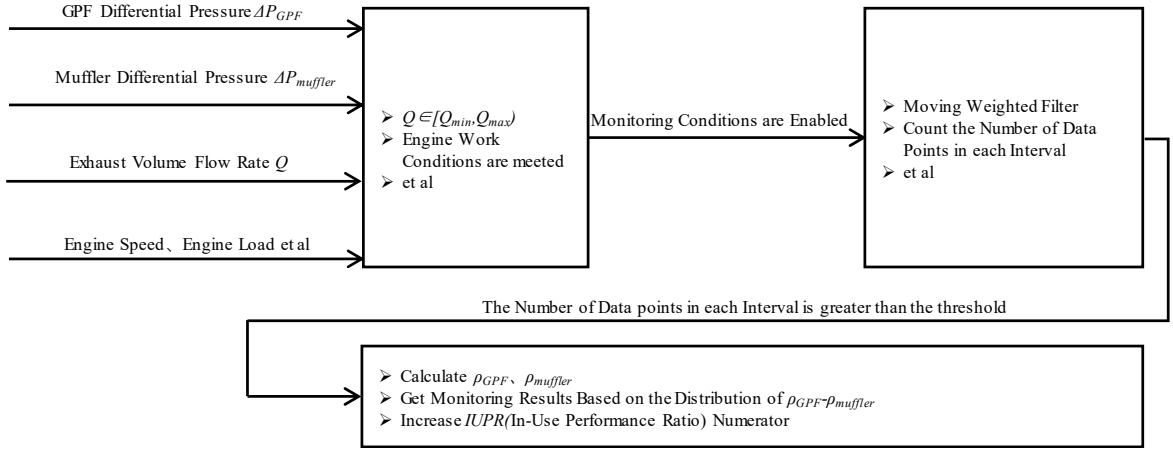

Figure 6. Monitoring Strategy Diagram.

First, as observed in Figures 3 and 4, the relative errors of the measured ΔP_{GPF} and $\Delta P_{muffler}$ are relatively large under operating conditions where the exhaust flow rate (Q) is small. However, the exhaust flow rate has an upper limit under the WLTC cycle. Therefore, the diagnostic function can be executed when the exhaust flow rate falls within a specific range [Q_{min}, Q_{max}). The specific range is [150 m^3/h,1150 m^3/h) in this pater.

Second, the range [Q_{min}, Q_{max}) is evenly divided into several sub-intervals (It has 50 sub-intervals in this paper). In the controller, the flow rate at the center of each sub-interval Q_i, the estimated GPF differential pressure corresponding to the central flow rate ΔP_{GPFi}, and the estimated muffler differential pressure $\Delta P_{muffleri}$ are stored separately.

When the exhaust flow rate falls within the corresponding sub-interval i, the currently measured differential pressures ΔP_{GPF} and $\Delta P_{muffler}$ are weighted and accumulated into the estimated differential pressure values at the center of this sub-interval in accordance with Equation (5).

$$\begin{cases} \Delta P_{GPFi}(n) = \big(1 - W(r)\big)\Delta P_{GPFi}(n-1) + W(r)\Delta P_{GPF} \\ \Delta P_{muffleri}(n) = \big(1 - W(r)\big)\Delta P_{muffleri}(n-1) + W(r)\Delta P_{muffler} \end{cases} \tag{5}$$

In the equation, $\Delta P_{GPFi}(n)$ denotes the estimated GPF differential pressure at the current moment for sub-interval i, $\Delta P_{GPFi}(n-1)$ denotes the estimated GPF differential pressure at the previous moment for sub-interval i, $\Delta P_{muffleri}(n)$ denotes the estimated muffler differential pressure at the current moment for sub-interval i, $\Delta P_{muffleri}(n-1)$ denotes the estimated muffler differential pressure at the previous moment for sub-interval i. $w(r)$ represents the weight function within the sub-interval, a commonly used Gaussian function is selected here, as shown in the Figure 7 below. r is the normalized distance between the current exhaust flow rate Q and the central flow rate Q_i of its corresponding sub-interval.

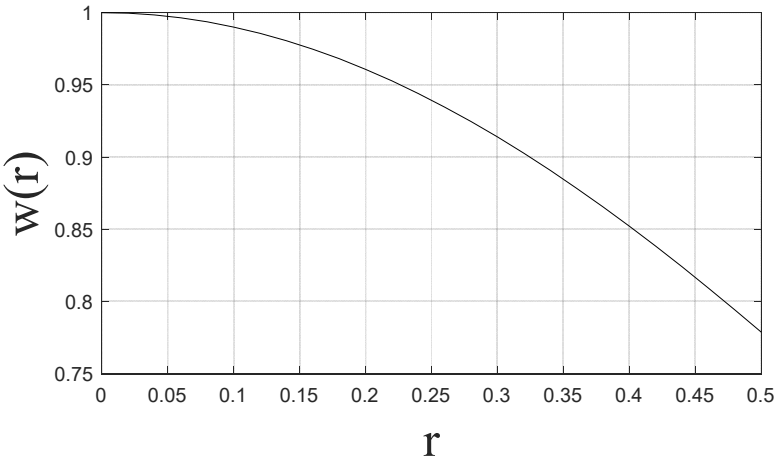

Figure 7. Gaussian Function.

When the number of updates for the estimated differential pressure values in the most of sub-intervals exceeds the set threshold (It is 20 in this paper), the Spearman's rank correlation coefficients ρ_{GPF} and $\rho_{muffler}$ can be calculated based on the latest estimated GPF differential pressure values $\Delta P_{GPFi}(n)$, latest estimated muffler differential pressure values $\Delta P_{mufflerI}(n)$, and exhaust flow rates Q_i at the sub-interval centers for each sub-interval. Subsequently, the presence of failures is determined according to the coordinate distribution range of ρ_{GPF}-$\rho_{muffler}$.

This method calculates the correlation coefficients only using the weighted average differential pressure values of each sub-interval and the exhaust flow rates at the sub-interval centers, thereby reducing the amount of data that needs to be stored during the diagnostic process. And also, it is applicable not only to conventional vehicles but also to hybrid vehicles, because it doesn't matter whether the engine operating condition is steady-state (hybrid vehicles) or dynamic (conventional vehicles). It's a statistical approach and is insensitive to data errors which is mentioned in Section 2.1 and this argument has been validated through the test results shown in next section.

4. Test Results with a PHEV (Plug-in Hybrid Electric Vehicle) Prototype-Vehicle

The aforementioned strategy was modeled and converted into code using MATLAB/SIMULINK, which was then integrated into an automotive-grade MCU. Subsequent WLTC cycle tests and real-road tests were conducted on a PHEV Vehicle, with the results presented in Figures 8–15. The key observations are as follows:

Within a single WLTC cycle test, 2 to 3 diagnostic procedures can be completed, and the scatter of the calculated ρ_{GPF} and $\rho_{muffler}$ values is small for each diagnostic run.

Under the GPF Normal Mode, the ρ_{GPF}-$\rho_{muffler}$ coordinates distribute in Range1, with no diagnostic trouble codes (DTCs) triggered.

Under the catastrophic GPF Mode, the ρ_{GPF}-$\rho_{muffler}$ coordinates distribute in Range3, and the diagnostic trouble code P226E00 (corresponding to the failure "Catastrophic GPF") can be triggered successfully.

During the real-road tests, tests for other failure modes were also conducted, and the diagnostic strategy was able to accurately identify the corresponding failure modes in all cases.

Figure 8. Normal GPF Test Results in WLTC.

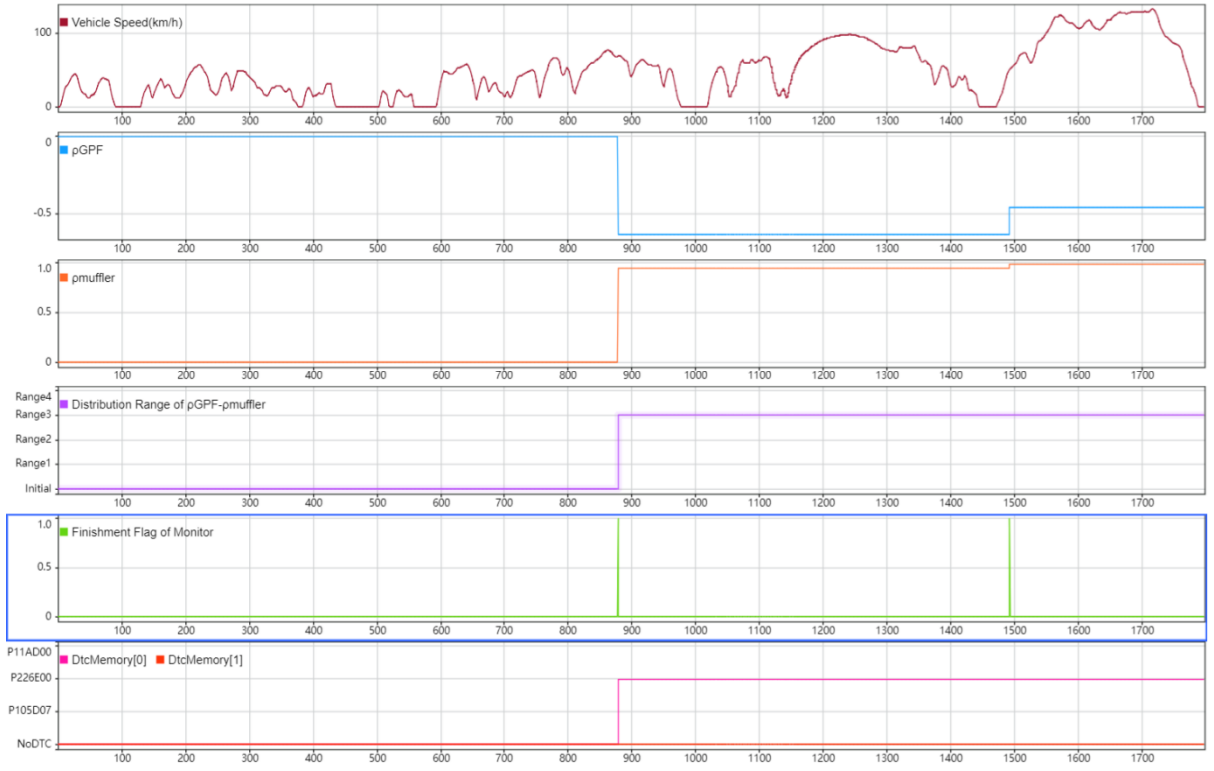

Figure 9. Catastrophic GPF Test Results in WLTC (P226E00).

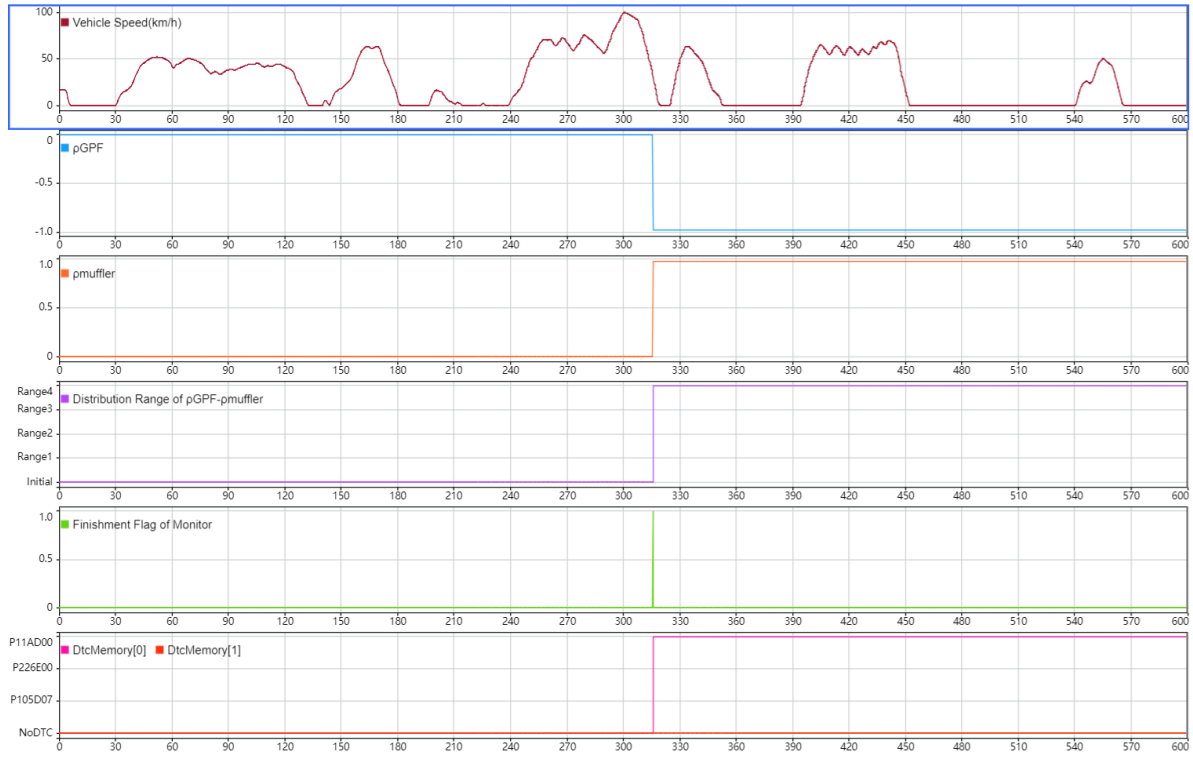

Figure 10. Upstream Hoseline Drop Off (P11AD00).

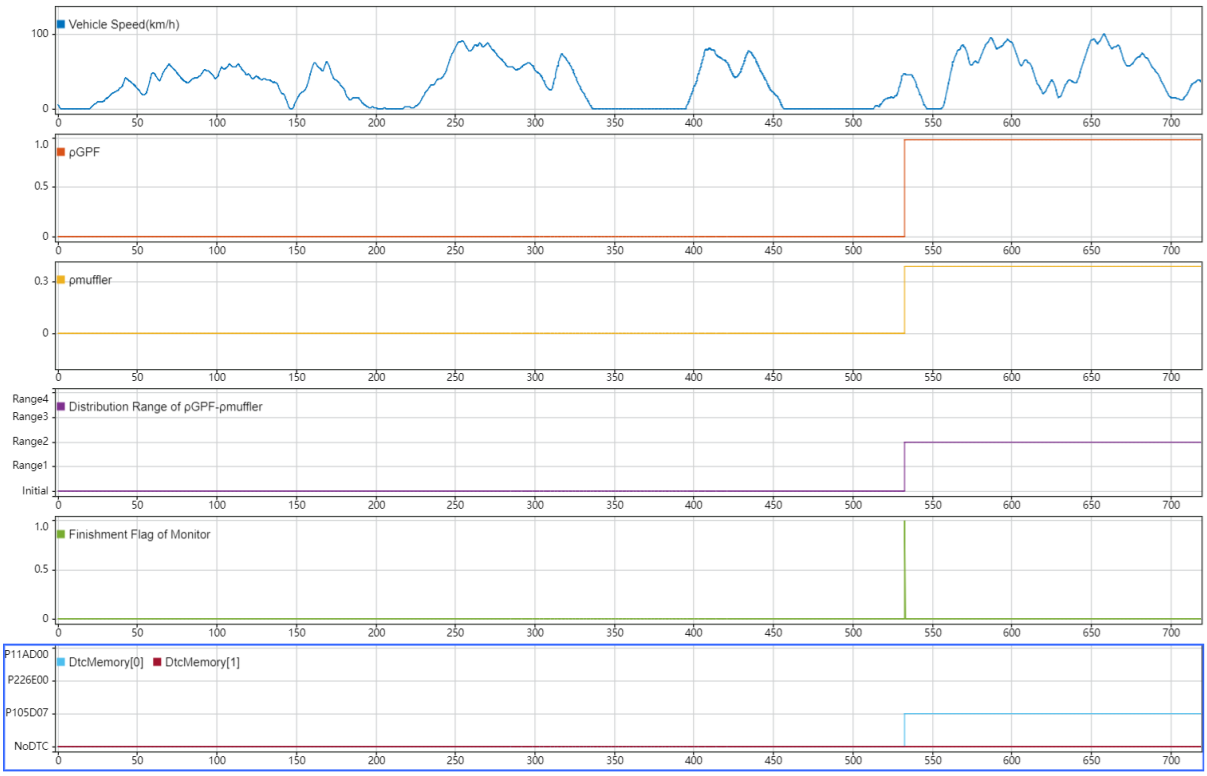

Figure 11. Downstream Hoseline Drop Off (P105D07).

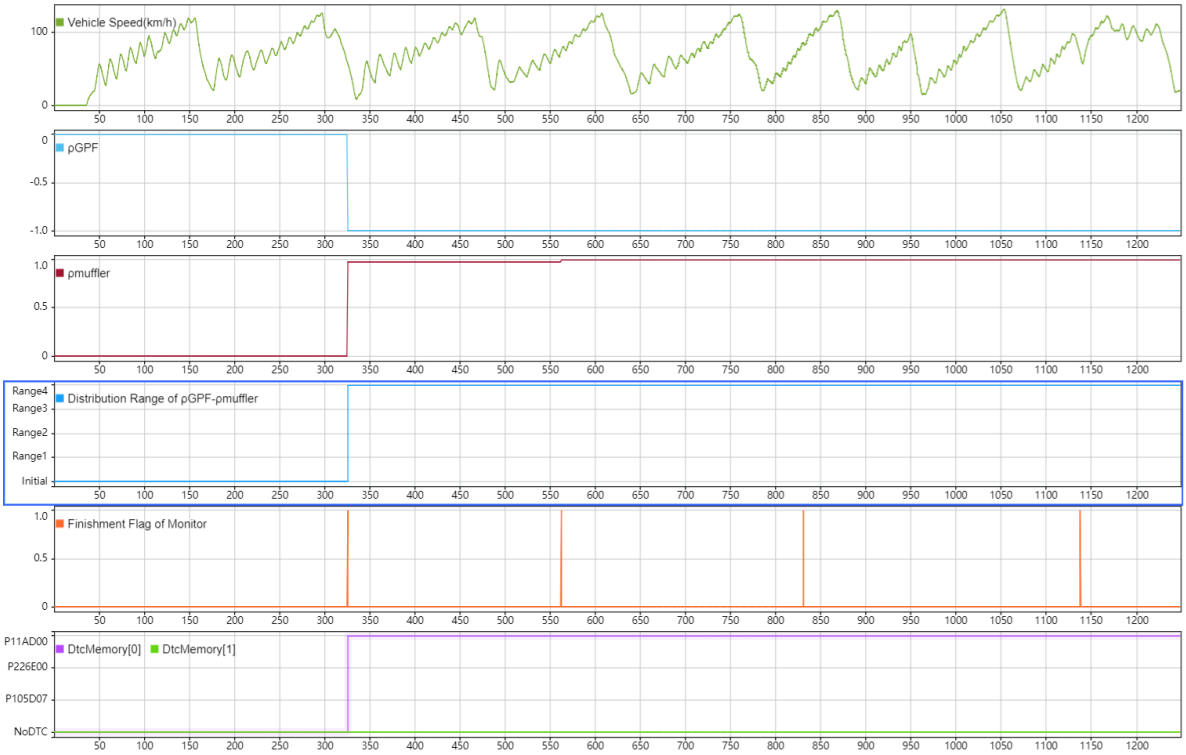

Figure 12. Hoseline Interchange (P11AD00).

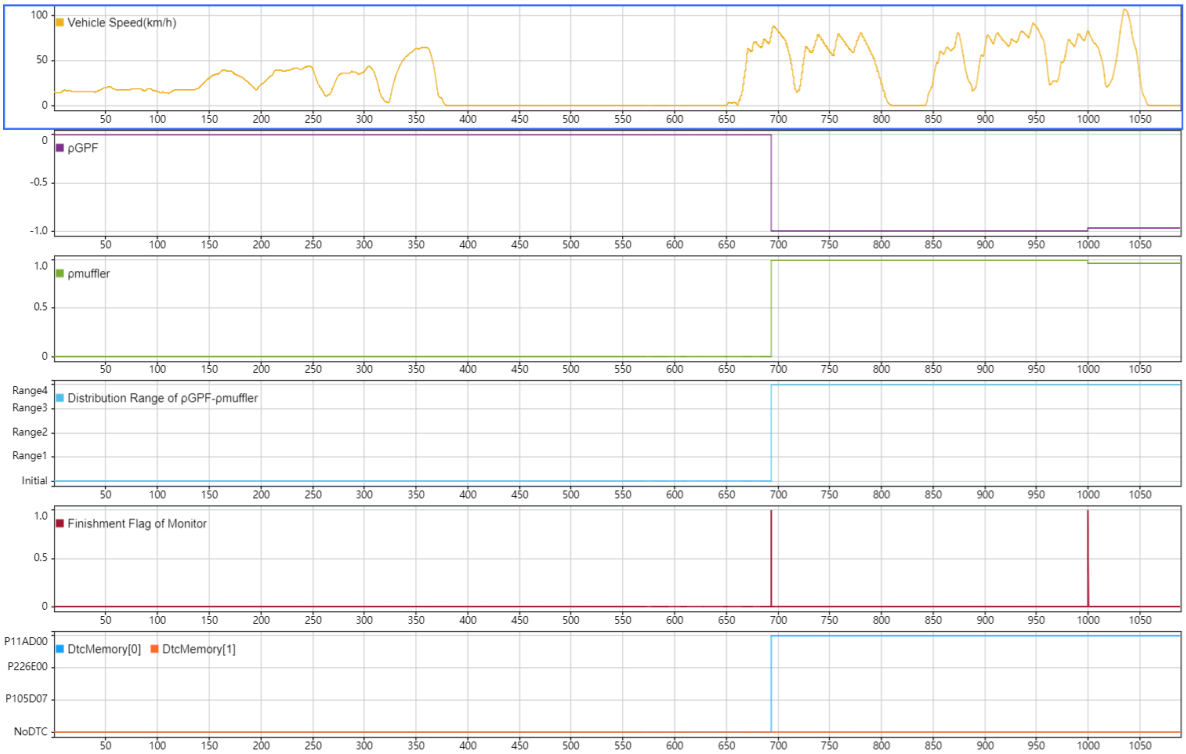

Figure 13. Catastrophic GPF & Upstream Hoseline Drop Off (P11AD00).

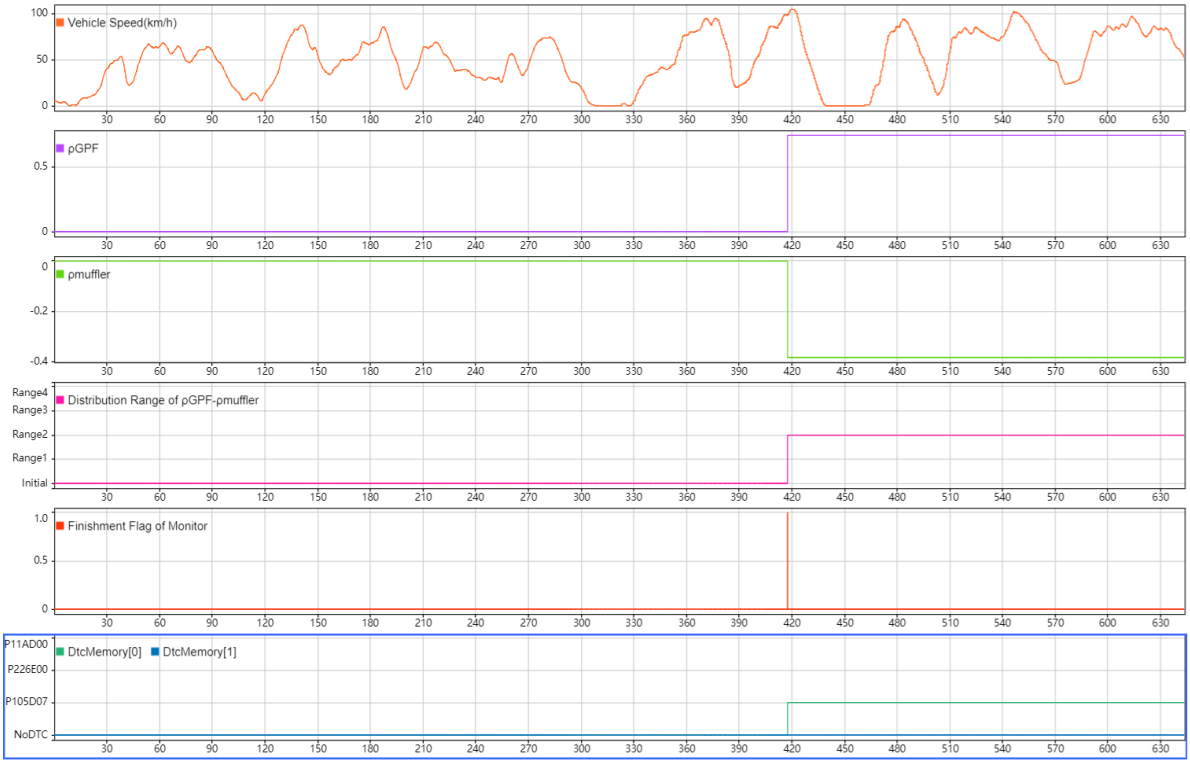

Figure 14. Catastrophic GPF & Downstream Hoseline Drop Off (P105D07).

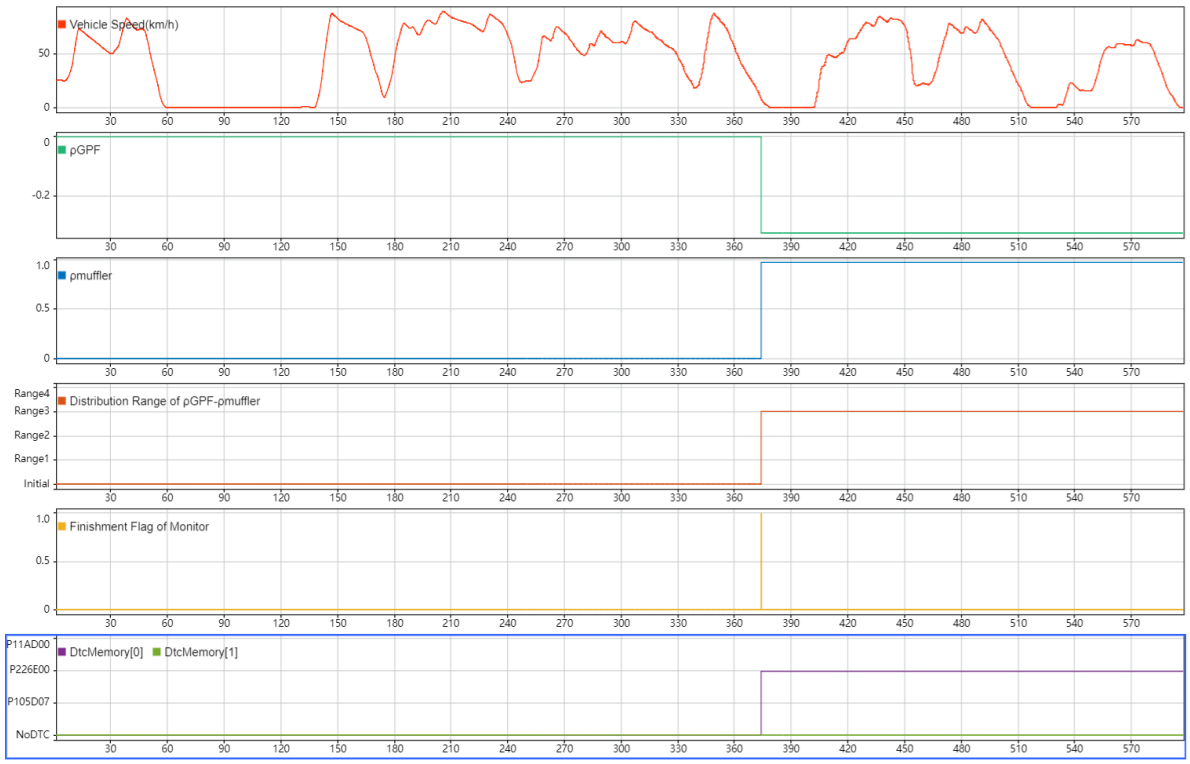

Figure 15. Catastrophic GPF & Hoseline Interchange (P226E00).

5. Conclusions

It is feasible to diagnose failure s such as GPF catastrophic failure and implausible GPF differential pressure signals by calculating the Spearman's rank correlation coefficient between GPF differential pressure and volume flow rate, as well as the Spearman's rank correlation coefficient between muffler differential pressure and exhaust

volume flow rate, and then utilizing the numerical distribution of these two correlation coefficients. This approach can meet the requirements of both product applications and OBD standards.

Through the simplified design of the diagnostic algorithm, this solution can be implemented on the actual vehicle ECU. Compared with the GPF diagnosis method based on differential pressure models, the diagnostic scheme proposed in this paper eliminates the need for calibration of the GPF differential pressure model, thereby reducing the workload of vehicle tests.

Author Contributions: N.D.: software, methodology, validation, investigation, visualization, writing—original draft; T.S.: validation, investigation, formal analysis, writing—review & editing; R.M.: investigation, writing—review & editing; P.S.: conceptualization, supervision, writing—review & editing; All authors have read and agreed to the published version of the manuscript.

Funding: This research received no external funding.

Institutional Review Board Statement: Not applicable.

Informed Consent Statement: Not applicable.

Data Availability Statement: Not applicable.

Conflicts of Interest: The authors declare no conflict of interest.

Use of AI and AI-Assisted Technologies: No AI tools were utilized for this paper.

References

1. Zhang, D.; Li, M.; Li, L.; Deng, J.; Li, Y.; Zhou, R.; Ma, L. Failure Analysis and Reliability Optimization Approaches for Particulate Filter of Diesel Engine after-Treatment System. *Int. J. Automot. Manuf. Mater.* **2025**, *4*, 2. https://doi.org/10.53941/ijamm.2025.100002.
2. Wang, Q.; Guo, B.; Zhong, W.; Jiang, P.; Liu, X. Study on Combustion and Soot Formation Characteristics of RCCI Engine with Diesel Mixed with PODE Ignited Gasoline. *Int. J. Automot. Manuf. Mater.* **2024**, *3*, 2. https://doi.org/10.53941/ijamm.2024.100002.
3. Bao, L.; Wang, J.; Shi, L.; Chen, H. Exhaust Gas After-Treatment Systems for Gasoline and Diesel Vehicles. *Int. J. Automot. Manuf. Mater.* **2022**, *1*, 9. https://doi.org/10.53941/ijamm0101009.
4. Tan, Y.; Kou, C.; Ning, D.; Feng, C. Effects of the structure parameters on methane emission control of an adsorptive three-way catalytic converter during cold start of the heavy-duty natural gas engines. *Energy* **2025**, *317*, 134654. https://doi.org/10.1016/j.energy.2025.134654.
5. E, J.; Zhou, H.; Kou, C.; Feng, C.; Zou, Z. Effect analysis on the hydrocarbon adsorption performance enhancement of the different zeolite molecular sieves in the gasoline engine under the cold start process. *Energy* **2024**, *305*, 132212. https://doi.org/10.1016/j.energy.2024.132212.
6. *GB18352.5-2016*; Limits and Measurement Methods for Emissions from Light-Duty Vehicles (CHINA VI). Ministry of Ecology and Environment of the People's Republic of China: Beijng, China, 2020.
7. *UN R83.07*; Uniform Provisions Concerning the Approval of Vehicles with Regard to the Emission of Pollutants according to Engine Fuel Requirements. UNECE: Geneva, Switzerland, 2017.
8. *13 CCR § 1968.2*; Malfunction and Diagnostic System Requirements—2004 and Subsequent Model-Year Passenger Cars, Light-Duty Trucks, and Medium-Duty Vehicles and Engines. California Air Resources Board: Sacramento, CA, USA, 2004.
9. Liu, Y.; Pan, J.; Lin, Y.; Zhang, Y.; Shuai, S.; Hua, L. Fault diagnosis of gasoline particulate filter based on neural network. *Automot. Engines* **2019**, 1–7.
10. Wang, P.; Xu, C.; Zhao, W.; Fan, L. Fault Diagnosis Strategy Function Development of Gasoline Particulate Filter in Compliance with China VI Regulation. *Chin. Intern. Combust. Engine Eng.* **2022**, *43*, 91–99.
11. Ojimah, A. Gasoline particulate filter (GPF) expansion/contraction pressure losses. *World J. Innov. Res.* **2018**, 5, 18–29.
12. Konstandopoulos, G.A.; Skaperdas, E.; Masoudi, M. Microstructural Properties of Soot Deposits in Diesel Particulate Traps. SAE Paper 2002-01-10. Available online: https://legacy.sae.org/publications/technical-papers/content/2002-01-1015/ (accessed on 4 January 2026).
13. Best, D.J.; Roberts, D.E. Algorithm AS 89: The Upper Tail Probabilities of Spearman's rho. *Appl. Stat.* **1975**, *24*, 377–379.